UILU-ENG 85-3603

Report No. 119

FATIGUE BEHAVIOR OF GRAY CAST IRON UNDER AXIAL AND BENDING LOADS

by

Peter J. Furman

Materials and Design Division
Department of Mechanical and Industrial Engineering

A Report of the

MATERIALS ENGINEERING - MECHANICAL BEHAVIOR

College of Engineering, University of Illinois at Urbana-Champaign

May 1985

ABSTRACT

Recent developments in characterizing low cycle ($<10^5$) fatigue behavior of gray cast iron were extended by investigating the effects of compressive mean stress. Axial fatigue tests were conducted with either tensile or compressive maximum stresses. A Manson-Halford formulation of the strain-life approach was found to be less effective for low cycle fatigue life prediction than a Smith, Watson, and Topper (SWT) combined stress-strain damage parameter. Fatigue lives from a wide range of axial loading conditions demonstrate good correlation using the SWT parameter.

Flexural fatigue behavior of gray cast iron was also investigated. Strain energy concepts were employed to predict stress-strain response of a beam under four-point bending. Fatigue lives were estimated from stress-strain predictions at the location of maximum stress. Strain gauge results from the bending tests indicated that strain energy concepts accurately predicted the beam deformation. Fatigue lives were accurately predicted by employing the damage parameter identified for axial loading.

ACKNOWLEDGMENTS

This investigation was conducted in the Materials Engineering Research Laboratory at the University of Illinois at Urbana-Champaign. Funding was provided by the Fracture Control Program.

I would like to thank Dr. Peter Kurath for many years of friendship and technical advice, Professor Darrell F. Socie for providing the freedom to develop professionally as well as technically, and June Kempka and the staff at the Department of Mechanical and Industrial Engineering Publications office for their excellent service in preparing this document.

All test materials were generously provided by Deere and Company, Moline, Illinois. D. L. Brodd is gratefully acknowledged for performing chemical and microstructural analyses.

Finally, the author would like to thank his wife, Judi, and children, Amanda and Lauren, for their encouragement and patience making this task most enjoyable.

TABLE OF CONTENTS

LIST OF TABLES

LIST OF FIGURES

NOMENCLATURE

A_{eff}	Cross-sectional area fraction unaffected by surface cracking
A_c, A_t	Area under compressive and tensile portion of stress-strain curve
b	Fatigue strength exponent
c	Fatigue ductility exponent
d	Beam dimensional constant
E	Linear modulus of elasticity
E_o	Tangent modulus at zero stress and strain
E_u	Unloading modulus from peak tensile stress
$f_\varepsilon(\sigma)$	Stress-strain function formulated as strain in terms of stress
$f_\sigma(\varepsilon)$	Stress-strain function formulated as stress in terms of strain
k	Monotonic strength coefficient
K_B	Bulk strength coefficient
K'	Cyclic strength coefficient
m	Slope of secant modulus versus stress curve
m_B	Bulk secant slope
n	Strain hardening exponent
n_B	Bulk strain hardening exponent
n'	Cyclic strain hardening exponent
$N_f, 2N_f$	Number of cycles, reversals to failure
N_p	Predicted cycles to failure
$N_{10\%}$	Number of cycles to 10% tensile load drop

q	Exponent of crack closure response
Q	Coefficient of crack closure response
R_σ	Stress ratio (maximum stress/minimum stress)
U_c, U_t	Compressive and tensile strain energies
ε	Strain
$\varepsilon_c, \varepsilon_t$	Maximum compressive, tensile strain for bending analysis
ε_f'	Fatigue ductility coefficient
ε_{max}	Maximum strain (absolute value)
ε_o	Mean strain
ε_R, ε_S	Remaining and secant strain
$\Delta\varepsilon/2$	Total strain amplitude
$\Delta\varepsilon_e/2$, $\Delta\varepsilon_p/2$	Elastic and plastic strain amplitudes
$\Delta\sigma/2$	Stress amplitude
σ	Stress
σ_B	Bulk stress
$(\sigma_B)_c$	Bulk stress in compression
σ_c, σ_t	Maximum compressive, tensile stress for bending analysis
σ_{cc}	Crack closure stress
σ_f'	Fatigue strength coefficient
σ_o	Mean stress
σ_G	Graphite constraint stress
$(\sigma_M)_c$	Monotonic compressive stress
σ_{max}	Maximum tensile stress
σ_u	Ultimate strength
ρ	Radius of curvature of the elastic line of a bent bar

1. INTRODUCTION

1.1 Background

Strain cycle fatigue data are often used in conjunction with the local strain approach [1,2]* for fatigue analysis in industrial design applications. Major features of the local strain approach are: (1) smooth specimen laboratory characterization of fatigue behavior for a given material [3]; (2) stress-strain simulation of a component at a critical location (e.g., stress concentration); (3) a technique for identifying damaging events within variable load histories; (4) a method to incorporate the mean stress effects into the damage algorithm; and (5) a damage summation technique for variable amplitude loading histories. Results of such analyses are considered to be fatigue crack initiation predictions for components. The success of these design methods has been demonstrated for wrought materials; however, applicability of these methods to cast iron has yet to be verified.

Uniaxial fatigue of cast iron has been the research topic of numerous investigators. Thum and Ude [4] modeled notch severity effects to show that the morphology of the free graphite phase governed material response. Gilbert [5] found that under tensile loading free graphite cracked and debonded, resulting in void formation. Fatigue cracks were found to initiate at flakes oriented normal to the loading direction. It is the presence of cracks and voids that causes cast iron's asymmetric stress-strain behavior. Ikawa and Ohira [6] and Mitchell [7] considered graphite phase size and shape effects on the fatigue resis-

* Numbers in brackets refer to REFERENCES following the text.

tance of various cast irons. Their results indicate that decreasing the microstructural notch severity improves fatigue performance. Gray cast iron, with its highly branched, interconnected graphite flake structure, displayed the lowest fatigue resistance. Using a surface replication procedure, Fash, et al. [8], observed that up to 95 percent of the fatigue life (i.e., specimen separation) of gray cast iron is spent in the growth, development, and linking of multiple crack systems.

In summary, the research conducted on low cycle fatigue behavior of gray cast iron points out that its failure mechanism is primarily crack growth. The use of crack initiation based design methods for cast iron components may be incorrect in the sense that these methods model a different failure mechanism. Many current design codes for cast iron components are based on procedures developed for wrought materials.

Recently, an improved gray cast iron fatigue analysis technique has been developed. Fash and Socie [9] have shown good results correlating their gray cast iron fatigue data with a bulk stress-strain parameter proposed by Smith, Watson, and Topper [10]. This parameter had been proposed to reflect early crack growth in fatigue. Socie, et al. [11], employed the Smith, Watson, and Topper (SWT) parameter in a nonlinear continuum damage approach to correctly predict the uniaxial fatigue life of gray cast iron under variable loading histories. Development of fatigue design procedures reflecting cast iron's actual damage mechanism are preferable to traditional design methods based on wrought material characteristics.

1.2 Purpose and Scope

In an attempt to extend recent fatigue analysis developments for gray cast iron, two topics were selected for further study. The first subject was the effect of high compressive mean stresses on uniaxial fatigue lives. This loading environment is common for structural applications of gray cast iron. Applicability of two strain-life parameters was explored for compressive mean stresses. The second topic investigated was the fatigue life analysis of a gray cast iron component using the SWT strain-life parameter. The "component" selected was a beam subjected to four-point bending. A monotonic stress-strain relationship developed by Downing [12] for cast iron was employed to predict beam deformation. Fatigue lives of the bending tests were estimated using a SWT relationship. Four-point bending was specifically chosen because it provides a simple linear strain gradient and also provides an opportunity to evaluate flexural fatigue behavior employing uniaxial data. Results from bending tests may be useful in assessing notched member response by indicating fatigue notch factor trends under linear strain gradients.

2. MATERIAL DESCRIPTION

2.1 Uniaxial Specimens

Uniaxial specimens (Fig. 1) were machined from test bars, 36 mm in diameter and 200 mm long, that were cast in chemically bonded sand molds to produce pearlitic gray iron. Graphite flake structure (Fig. 3) was classified [13] as primarily Type A (sizes 3 and 4) with some Type D. Matrix microstructure was classified as lamillar pearlite with 1 to 2 percent free ferrite. Material chemistry is given in Table 1. Monotonic stress-strain properties are listed in Table 4.

2.2 Bending Specimens

Bending specimens were cast near net shape and machined into the square bars illustrated in Fig. 2. Graphite flake structure (Fig. 4) was classified as primarily Type A (sizes 3 and 4) with traces of Type E. Matrix microstructure was lamillar pearlite with very slight traces of free ferrite and steadite. Chemistry is presented in Table 1 and stress-strain properties in Table 4.

3. COMPRESSIVE MEAN STRESS EFFECTS

3.1 Introduction

Any relationship developed to characterize fatigue behavior must have its limit of applicability defined. An examination of Fash and Socie's [9] data, used in determining the effect of mean stress on fatigue behavior for gray cast iron, revealed a lack of high compressive mean stress results. To clarify the applicable range for SWT parameter implementation, compressive mean stress fatigue tests were conducted. The investigation included tests with tensile and compressive maximum stresses. A general form of the SWT parameter is

$$N_f \propto \sqrt{\sigma_{max}\,\Delta\varepsilon/2} \quad . \tag{1}$$

Compressive maximum stresses cause the SWT parameter to become undefined. Possible evaluation of this stress state as a nondamaging fatigue condition was explored. Finally, evaluation of gray cast iron fatigue data by both the SWT and Manson-Halford strain-life relationships was performed to identify the superior method for incorporation in a design procedure.

3.2 Testing Program

A Goodman diagram for gray cast iron (Fig. 5) was divided into three distinct zones for the purpose of discussion. Region I represents the combination of alternating and mean stresses that exceed the ultimate strength for gray iron in either tension or compression. This region is considered to be unavailable for fatigue testing. Regions II

and III are feasible for fatigue testing. Region III is separated because the combination of stresses result in the maximum stress being equal to or less than zero (i.e., σ_{max} is compressive). To demonstrate the effect of compressive mean stress on gray cast iron's fatigue behavior, tests were conducted in both regions II and III.

All testing was completed on a 20 kip MTS servo-hydraulic test frame. Test control, whether strain or load, was achieved by the use of either a multi-user or dedicated single board computer. Digital stress-strain data was recorded periodically for each test. Results from the uniaxial compressive mean stress fatigue tests are presented in Table 2.

3.3 Analysis-Mean Stress Correlation Techniques

3.3.1 SWT Parameter

Fash and Socie selected a form of the SWT parameter in which the maximum stress was multiplied by the strain amplitude. They found their fatigue data was best correlated by the following relationship:

$$\sigma_{max}(\Delta\varepsilon/2) = C(N_f)^{\beta} \quad . \qquad (2)$$

Figure 6 displays the results of approximately 50 fatigue tests [9] conducted in either strain or load control. Although the constants for Eq. (2) were determined by regression analysis for all the tests, similar values resulted from analyzing only the completely reversed strain control fatigue tests. The SWT relationship displays insensitivity to the choice of either "stabilized" half-life or initial stress-strain response. This is attributed to the gradual and constant degradation of

load observed in strain control, or strain amplitude increase in load control. Fash and Socie's investigation demonstrated that cast iron fatigue tests conducted in either strain or load control, with or without mean values, can be correlated by a single relationship.

3.3.2 Manson-Halford Relationship

Although the SWT parameter has been shown to successfully correlate cast iron fatigue data, other mean stress correction techniques are frequently employed. The strain-life relationship, ignoring the effect of mean stress, is often presented as

$$\frac{\Delta\varepsilon}{2} = \frac{\Delta\varepsilon_e}{2} + \frac{\Delta\varepsilon_p}{2} = \frac{\sigma_f'}{E}(2N_f)^b + \varepsilon_f'(2N_f)^c \quad . \qquad (3)$$

The fatigue constants σ_f', ε_f' b, and c are determined from the results of completely reversed strain controlled tests [3]. Morrow [14] suggested that the effect of mean stress on high cycle fatigue can be accounted for by modifying Basquin's equation [15]

$$\frac{\Delta\varepsilon_e}{2} = \frac{\Delta\sigma}{2E} = \frac{(\sigma_f' - \sigma_o)}{E}(2N_f)^b \quad . \qquad (4)$$

Manson and Halford [16] modified the strain-life equation to include the effects of mean stress. The elastic portion of Eq. (3) was altered as suggested by Morrow, while the plastic portion was changed to maintain the ratio of elastic to plastic strains as dictated by the stress-strain response.

The following equation results:

$$\frac{\Delta\varepsilon}{2} = \frac{\Delta\varepsilon_e}{2} + \frac{\Delta\varepsilon_p}{2} = \frac{\sigma_f' - \sigma_o}{E}(2N_f)^b + \varepsilon_f'\left(\frac{\sigma_f' - \sigma_o}{\sigma_f'}\right)^{c/b}(2N_f)^c \quad . \quad (5)$$

The preceding formulations all assume that stress-strain response can be characterized by a Ramberg-Osgood relationship:

$$\frac{\Delta\varepsilon}{2} = \frac{\Delta\varepsilon_e}{2} + \frac{\Delta\varepsilon_p}{2} = \frac{\Delta\sigma}{2E} + \left(\frac{\Delta\sigma'}{2K'}\right)^{1/n'} \quad . \quad (6)$$

This type of representation is inaccurate for gray cast iron due to its lack of an initial linear elastic response. Downing found that monotonic stress-strain simulation was accurately modeled by considering a linear variation in secant modulus. A component of total strain, termed the secant strain, ε_s, was calculated from the secant modulus. The remaining strain, ε_R, was formulated in the same manner as plastic strain for wrought materials:

$$\varepsilon = \varepsilon_s + \varepsilon_R = \frac{\sigma}{E_o + m\sigma} + \left(\frac{\sigma}{k}\right)^{1/n} \quad . \quad (7)$$

Asymmetric stress-strain behavior of cast iron was incorporated into Eq. (7) by allowing m and k to have different values for tension and compression. In order to determine the fatigue constants for use in Eq. (5), the elastic and plastic strain contributions were calculated from the first and second terms of Eq. (7), respectively. Completely reversed strain control fatigue data from Fash and Socie were used to generate the fatigue constants (Fig. 7).

3.4 Results and Discussion

In order to illustrate the differences in fatigue life predictions for the SWT parameter and Manson-Halford relationships, a Goodman diagram with lines of constant life was constructed. In the construction of these lines, stress amplitude and mean stress values were selected throughout Region II of Fig. 5. Corresponding strain amplitudes were determined by simulating the stress-strain response. A cyclic response algorithm, developed by Downing [12], was employed in these simulations (a synopsis of his approach is presented in APPENDIX I).

Results of this comparison are graphically depicted in Fig. 8. Significant differences in the predictions are apparent at fatigue lives greater than 10^3 cycles. For tensile mean stresses, the SWT parameter predicts a larger number of cycles to failure than the Manson-Halford strain-life method. Conversely, compressive mean stresses cause the Manson-Halford method to predict longer fatigue lives than the SWT parameter.

The effectiveness of the two mean stress modifications is illustrated by comparing predictions of fatigue life to experimental results. Completely reversed and tensile mean fatigue data from Fash and Socie, as well as current data reflecting high compressive mean stress effects, were used in the comparison. Figure 9 illustrates the results of SWT parameter implementation. The data are correlated within a factor of two for the majority of the low-cycle fatigue tests. SWT fatigue life predictions greater than 10^5 cycles are observed to be conservative with regard to experimental results. The Manson-Halford

relationship does not predict the experimental trends as effectively as the SWT parameter over the life ranges tested (Fig. 10).

Figure 11 demonstrates the range of SWT parameter applicability. Test results with zero, high tensile, and high compressive mean stresses are all predicted by a single relationship. The stress ratio, R_σ, of Fash and Socie's data ranged from -1.67 to 0.5. Current tests incorporate results for R_σ ranging from $-\infty$ to 5.9.

The cyclic stress-strain response of tests with compressive maximum stresses (Region III) is illustrated in Figs. 12 and 13. Though cyclic creep was observed in the load controlled test and mean stress relaxation occurred in strain control, testing was halted in both cases after 10^7 cycles because specimen failure did not occur. Microscopic examination of surface replicas, taken upon conclusion of testing, revealed no signs of crack formation. These results indicate that region III conditions may be interpreted as non-damaging. The Manson-Halford relationship predicts a finite life for the tests conducted of approximately 7 x 10^6 cycles.

Use of the SWT parameter, as suggested by Fash and Socie, was found to be appropriate for previously uninvestigated loading conditions. This parameter suggests that tensile stress levels detrimentally affect the fatigue life of gray cast iron. Data from high compressive mean stress fatigue tests that have maximum tensile stresses greater than 50 MPa ($\sigma_{max}/\sigma_u < 0.2$) were correlated by the same relationship that was effective on previous data. Very low tensile stress levels ($\sigma_{max}/\sigma_u < 0.2$), which resulted in long life fatigue tests, were not predicted accurately by the SWT parameter. Fatigue cracks did not appear to initi-

ate as quickly in high cycle fatigue tests as cracks observed in tests with higher tensile maximum stresses. This phenomenon may be due to an absence of debonding between the matrix material and the graphite flakes at lower maximum stress levels. Cyclic tests performed under fully compressive stress excursions did not exhibit the cracking behavior that is characteristic of gray cast iron.

Crack propagation dominates gray cast iron's low cycle fatigue life. The success of the SWT parameter, when correlating fatigue life, may be due to its bulk stress-strain terms more accurately modeling the driving force for crack propagation. Traditional formulations of strain-life fatigue prediction methods are appropriate for materials which experience crack initiation caused by a slip damage process. Cast iron has been shown to be defect dominated, and crack initiation was altered by these defects.

4. BENDING

4.1 Background

General fatigue design procedures are often developed from information gained studying uniaxial behavior of materials. Recent gray cast iron research has provided useful tools for evaluation of stress-strain response and fatigue life behavior. In this study, the accuracy of these uniaxial relationships was evaluated in the prediction of stress-strain and fatigue behavior of a gray cast iron beam under four-point bending. Four-point bending provides a linear strain gradient, constant moment, and zero shear stress throughout the gauge (center) section of the beam. Elimination of shear stress should not affect fatigue life, because normal stresses were previously found to dominate fatigue damage accumulation in gray cast iron.

4.2 Testing Program

A four-point bending fixture (Fig. 14) was designed employing standard closed loop servo-hydraulic control. Loading conditions for each bending specimen were calculated to produce a completely reversed load, $R_\sigma = -1$, at the top surface of the beam. Results from eight bending fatigue tests are presented in Table 3. Three specimens were strain gauged to verify moment-strain predictions and outer fiber strain distribution.

4.3 Flexural Stress-Strain Analysis

Prediction of fatigue behavior for a cast iron beam must incorporate an analysis of its stress-strain response under bending.

Cast iron's asymmetric and non-linear stress-strain behavior precludes the use of standard strength of material solutions for stress, strain, or moment calculations. This asymmetry causes the neutral axis to shift away from the geometric center line during bending. The basic assumptions, however, remain the same.

1. The beam is straight and prismatic, with constant cross-sectional area.
2. Loading forces are directed perpendicular to the longitudinal axis.
3. Plane sections remain plane, resulting in a linear strain distribution.
4. The stress-strain model formulated from axial testing applies to flexural behavior.

The validity of these assumptions has been demonstrated by Bach [17] for materials which do not obey Hooke's law and possess no straight-line stress-strain curve for tension or compression. Meyer [18] also confirmed these assumptions for wrought iron undergoing plastic deformation. Relying on these assumptions and the derivation of plastic bending of bars with rectangular cross-sections, Nadai [19] wrote the static equilibrium equations as

$$\int_{-\varepsilon_c}^{\varepsilon_t} f_\sigma(\varepsilon)\, d\varepsilon = 0 \quad . \tag{8}$$

This equation states that the area under the stress-strain curve, or strain energy, for the tensile portion of the beam equals the strain energy for the portion subjected to compression (Fig. 15).

Separation of Eq. (8) into tensile and compressive contributions yields

$$U_t = A_t = \int_0^{\varepsilon_t} f_\sigma(\varepsilon)d\varepsilon \qquad (9)$$

and

$$U_c = A_c = \int_{-\varepsilon_c}^{0} f_\sigma(\varepsilon)d\varepsilon \quad . \qquad (10)$$

The equilibrium condition may be written as

$$U_t + U_c = 0 \quad . \qquad (11)$$

Nadai presented the bending moment in the following form:

$$M = d\rho^2 \int_{-\varepsilon_c}^{\varepsilon_t} f_\sigma(c)c \; dc \quad . \qquad (12)$$

Unfortunately, a closed form solution for strain energy could not be obtained since Downing's monotonic stress-strain formula, Eq. (7), was chosen to model deformation response:

$$\varepsilon = \frac{\sigma}{E_o + m\sigma} + \left(\frac{\sigma}{k}\right)^{1/n} \quad . \qquad (13)$$

The stress cannot be formulated explicitly in terms of strain; therefore, Eqs. (9), (10), and (12) cannot be solved directly. However, a closed form solution may be obtained using complementary strain

energy. The complimentary strain energy representations of Eqs. (9) and (10) are

$$U_t = A_t = \sigma_t \varepsilon_t - \int_0^{\sigma_t} f_\varepsilon(\sigma) d\sigma \qquad (14)$$

and

$$U_c = A_c = \sigma_c \varepsilon_c - \int_{-\sigma_c}^{0} f_\varepsilon(\sigma) d\sigma \quad . \qquad (15)$$

This formulation resulted in a closed form solution for the stress and strain distribution throughout the beam cross-section.

Tensile strain energy was determined for a value of maximum tensile stress and its corresponding strain. Compressive stress values were iteratively selected and compressive strain energy calculated until an equilibrium solution ($U_t + U_c = 0$) was identified. Stress-strain distributions were easily inferred from the linear strain gradient (Fig. 16). The moment was numerically calculated by dividing the stress distribution through the cross-section into small segments and multiplying by the appropriate moment arm. Moment-stress and moment-strain results from these calculations are graphically depicted in Fig. (17).

4.4 Results and Discussion

Due to differences in stress-strain response of the material used in the axial and bending sections of this investigation, results from Section 3 could not be employed to predict flexural fatigue lives. Strain life fatigue data from a gray iron with a monotonic response was

similar to the beam iron was used for life predictions (see APPENDIX II). A single, constant amplitude, load controlled, axial fatigue test conducted on the beam material correlated well with the fatigue data selected. Figure 18 illustrates the results of a SWT parameter fit to the fatigue data.

Deformation response under bending was calculated from the monotonic stress-strain behavior of the beam material. A comparison of actual and predicted bending response of a gray iron beam is presented in Fig. 19. Fatigue lives were estimated from calculated stress and strain amplitudes at the beam outer surface. Predicted cyclic strain levels displayed less than 5 percent deviation from actual moment-strain hysteresis loops obtained from two strain gauged beams (Fig. 20). Outer fiber surface strains were observed to vary less than 4 percent across the beam gauge section. Bending fatigue results are illustrated in Fig. 21 along with the SWT uniaxial relationship. Figure 22 shows that bending fatigue lives were predicted within a factor of two. These results indicate that beam deformation was accurately modeled by the strain-energy method, and the strain gradient had little impact on fatigue life.

Accurate prediction of bending fatigue lives from surface deformation behavior was attributed to the following factors: (1) the majority of gray cast iron's low cycle fatigue life comprises propagation of multiple surface cracks; and (2) a nearly constant stress field existed to the depth at which fatigue cracks were found to grow before fracture occured. A beam fracture surface photograph (Fig. 23) clearly indicates the depth to which the fatigue cracks grew. Crack

fronts were observed to be nearly linear across the fracture surface. The nearly constant stress gradient resulted from a combination of cast iron's non-linear stress-strain response and the geometry of the beam investigated. The strain gradient produced by this beam geometry was not particularly severe. A smaller beam would have a more severe gradient, decreasing the depth of the constant stress field, and resulting in increased interaction with fatigue cracks growing into the beam. Figure 16 illustrates the stress gradient produced from the combination of stress-strain response and geometric characteristics.

Fatigue notch sensitivity factors near unity were indicated for the geometry and load levels investigated. Small surface casting defects were present on a few of the beams tested but had a minimum effect on fatigue life. Stress concentrations from these casting defects did not significantly alter the dominance of gray cast iron's graphite flake microstructure. In contrast, nodular cast iron, whose microstructural notch severity is less severe, may be more sensitive to surface defects.

Flexural fatigue tests were not conducted for high cycle fatigue conditions. Life estimations for high cycle fatigue may not have the same degree of accuracy exhibited in the present investigation. This may be due to the lack of high cycle fatigue data correlation for the SWT parameter. Also, lower stress levels produce a stress gradient near the tensile surface. Fatigue cracks would spend a larger portion of life propagating into the nonuniform stress and strain gradients present. These factors reflect the differences reported in the literature between rotating beam and axial fatigue data.

5. CONCLUSIONS

Progress has been made toward developing design guidelines for gray cast iron components. The following conclusions have either been confirmed by, or drawn from this investigation:

1. Crack growth dominates gray cast iron's low cycle fatigue life.
2. Downing's deformation model formulated for cast iron accurately simulates uniaxial stress-strain response.
3. The Smith, Watson, and Topper (SWT) parameter was shown to correlate uniaxial low cycle fatigue data more accurately than a Manson-Halford strain-life approach. Conceptually, the SWT parameter may be more appropriate for characterization of low cycle fatigue behavior due to its bulk stress-strain terms more accurately modeling the driving force for crack propagation.
4. For high cycle fatigue ($>10^5$ cycles) where the failure mechanism is not dominated by crack growth, neither the SWT nor Manson-Halford approach successfully predicts fatigue lives.
5. High compressive mean stress fatigue tests having tensile maximum stress levels were predicted by the same SWT formulation that successfully correlated fully reversed testing.
6. The fully compressive cyclic tests ($\sigma_{max} < 0$) conducted in this investigation exhibited no fatigue damage after 10^7 cycles. The SWT relationship may be interpreted such that an event identified at these stress levels may be considered to be non-damaging. Fatigue testing at higher compressive stress levels may reveal shear type failure behavior.

7. Flexural deformation was accurately modeled with Downing's non-linear stress-strain formula. A complementary strain energy technique was employed to accurately predict for equilibrium stress and strain distributions in the beam.
8. Flexural fatigue data were successfully correlated employing surface deformation behavior of the beam in conjunction with a SWT relationship.

Table 1. Material Chemistry

Sample	C	Mn	P	S	Si	Ni	Cr	Mo	Cu
Uniaxial Specimen	3.34	0.37	0.013	0.023	1.96	0.08	0.05	0.01	0.34
Bending Specimen	3.54	0.42	0.038	0.060	2.18	0.11	0.17	0.03	0.10

Hardness

Uniaxial Specimen	207 BHN
Bending Specimen	212 BHN

Table 2. Compressive Mean Stress Fatigue Testing Results

Specimen No.	$\Delta\varepsilon/2$	ε_o	$\Delta\sigma/2$ (mPa)	σ_o (mPa)	N_f (cycles)
2	0.0025	-0.0025	-	-	$>1.00 \times 10^7$
3	0.0020	-0.0020	-	-	1.72×10^3
4	0.0010	-0.0080	-	-	$>1.00 \times 10^7$
5	-	-	142.	-200.	$>1.00 \times 10^7$
6	-	-	170.	-170.	$>1.00 \times 10^7$
7	-	-	200.	-142.	$\tilde{1}.00 \times 10^7$
8	0.0015	-0.0045	-	-	$>1.00 \times 10^7$
9	-	-	190.	-150.	$>1.00 \times 10^7$
10	-	-	185.	-130.	2.22×10^6
11	-	-	210.	-155.	2.86×10^5
12	-	-	230.	-170.	6.99×10^4

Table 3. Bending Fatigue Results

Specimen No.	$\Delta M/2$ (N-m)	M_o (N-m)	$\Delta\sigma/2$ (MPa)	Nf (cycles)
3	249	6	90	910,010
4	610	68	200	820
5	277	7	100	514,520
6	429	23	150	4,900
7	689	90	220	160
8	367	17	130	3,460
9	367	17	130	64,270
10	463	34	160	8,050

Table 4. Stress-Strain Properties

	Uniaxial Specimen	Bending Specimen
Elastic Tangent Modulus, E_o	119,550	119,550
Tensile Secant Slope, m_T	-200	-200
Tensile Strength Coefficient, k_T (MPa)	430	500
Tensile Hardening Exponent, n_T	0.115	0.115
Compressive Secant Slope, m_C	-100	-100
Compressive Strength Coefficient, k_C (MPa)	820	870
Compressive Hardening Exponent, n_C	0.115	0.115

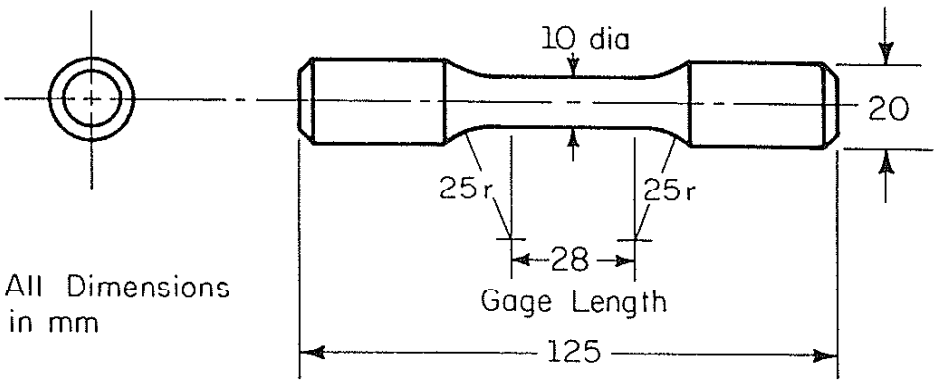

Figure 1. Uniaxial Test Specimen

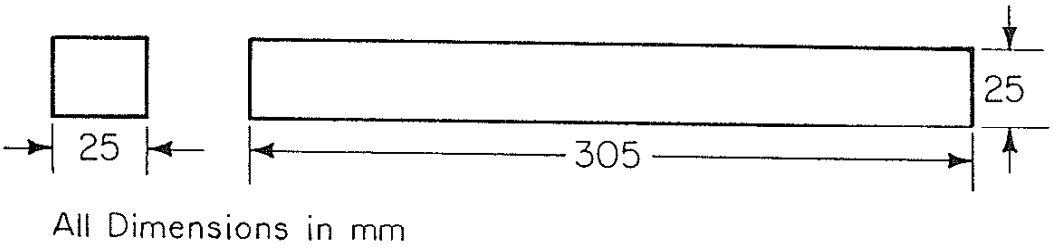

Figure 2. Bending Specimen

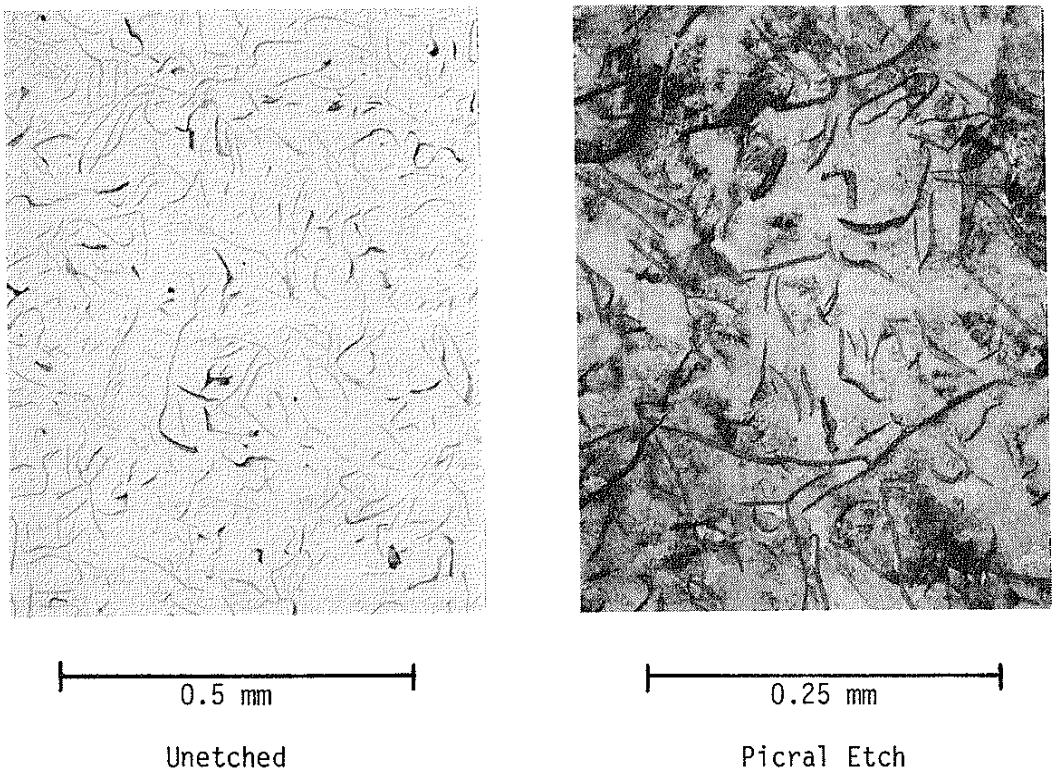

Figure 3. Uniaxial Specimen Microstructure

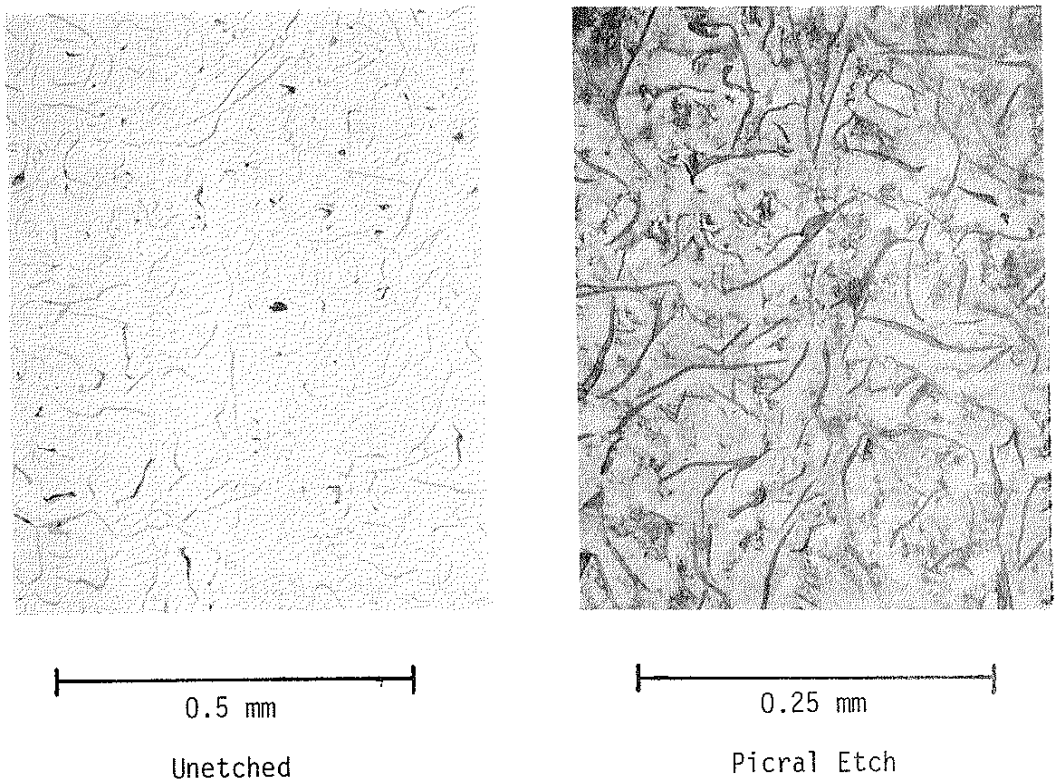

Figure 4. Bending Specimen Microstructure

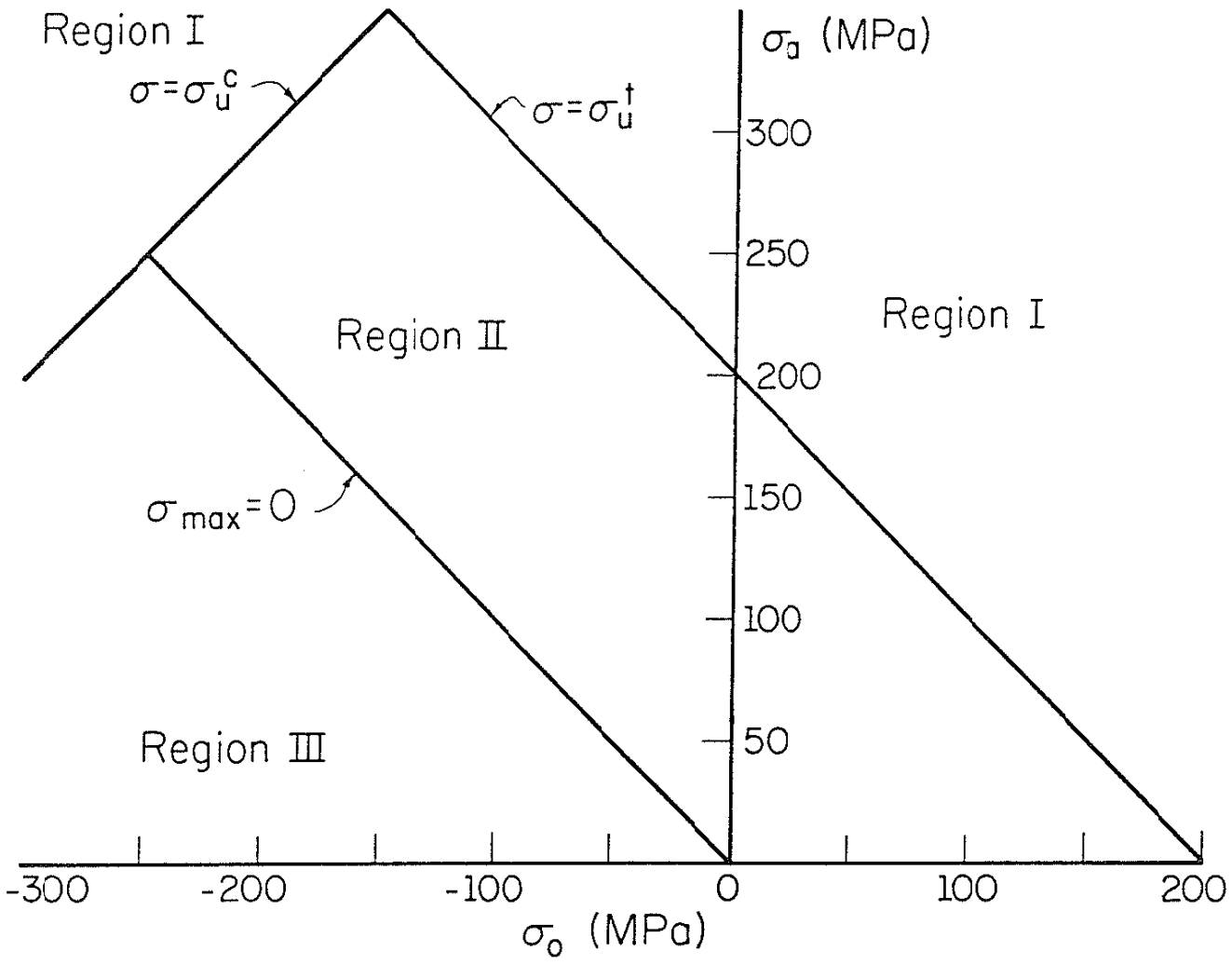

Figure 5. Proposed Testing Regions for Gray Cast Iron

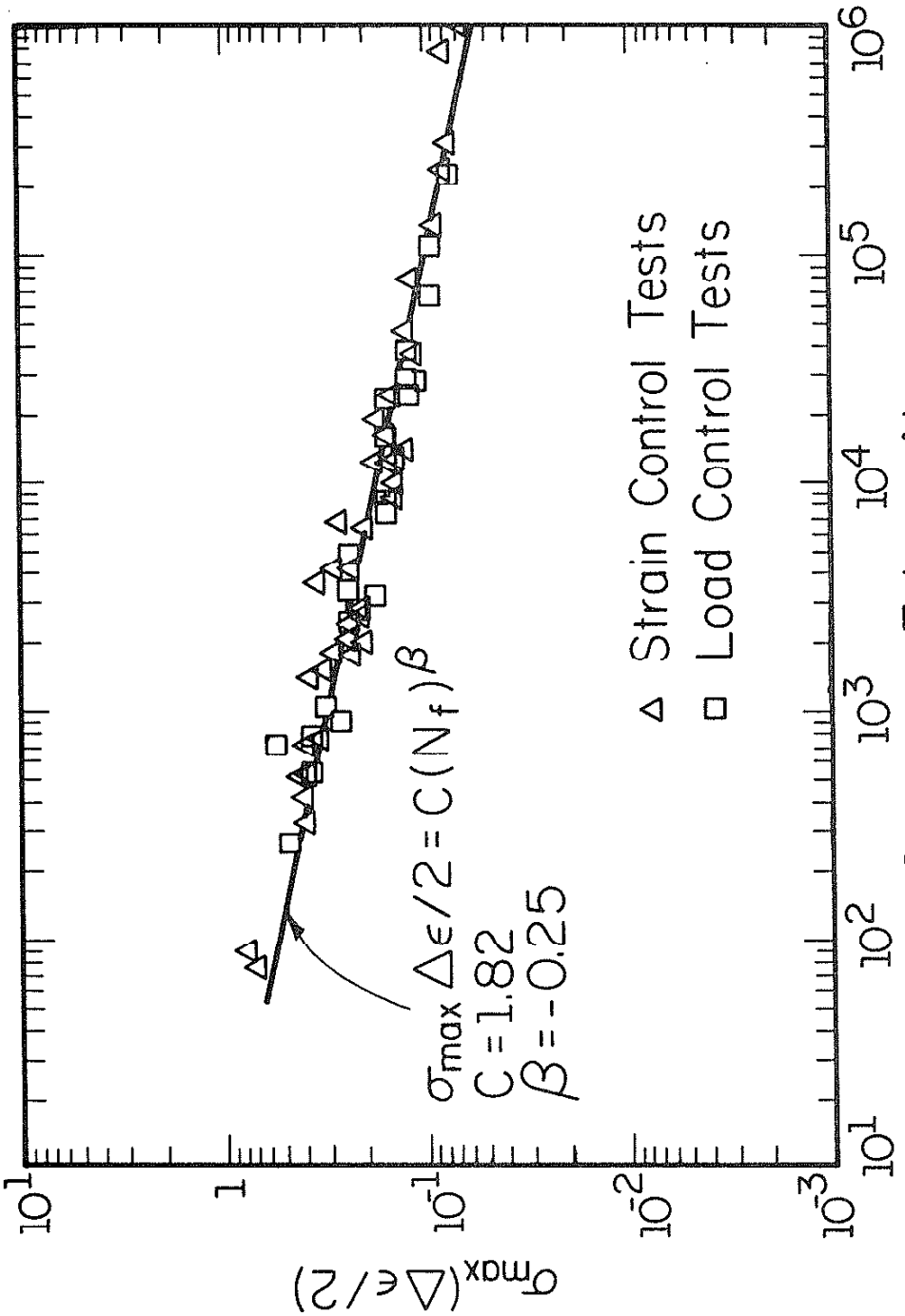

Figure 6. Fash and Socie Fatigue Testing Results

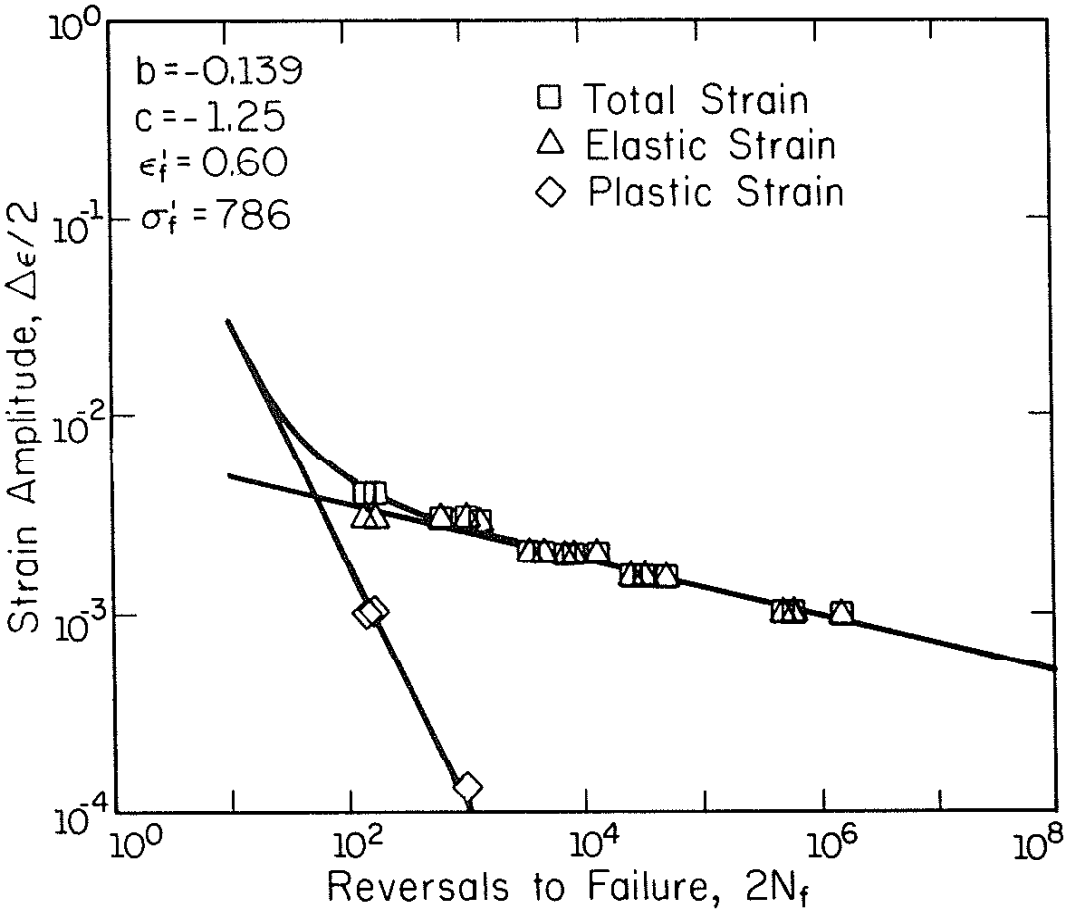

Figure 7. Strain-Life Fatigue Data

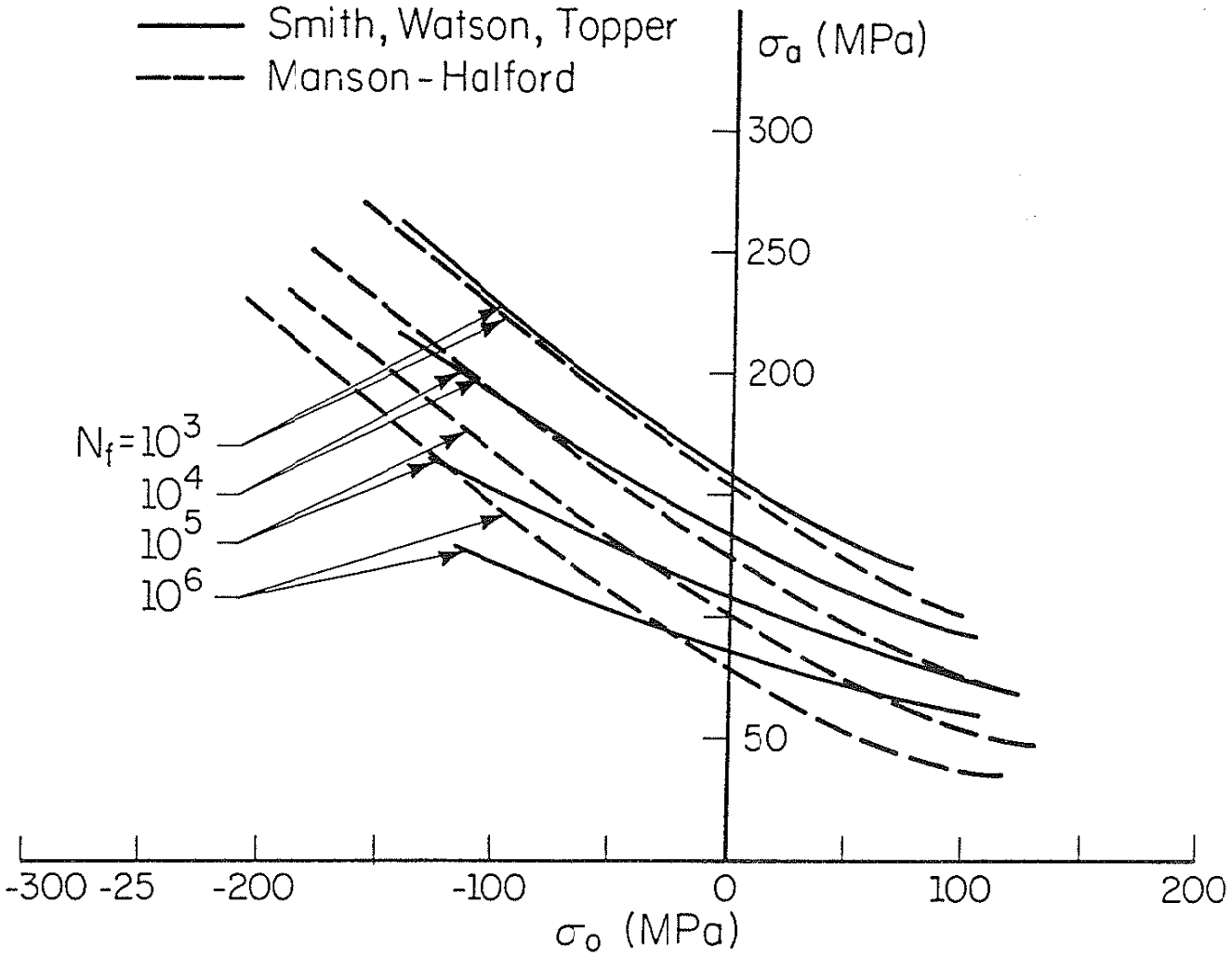

Figure 8. SWT and Manson-Halford Fatigue Life Prediction Trends

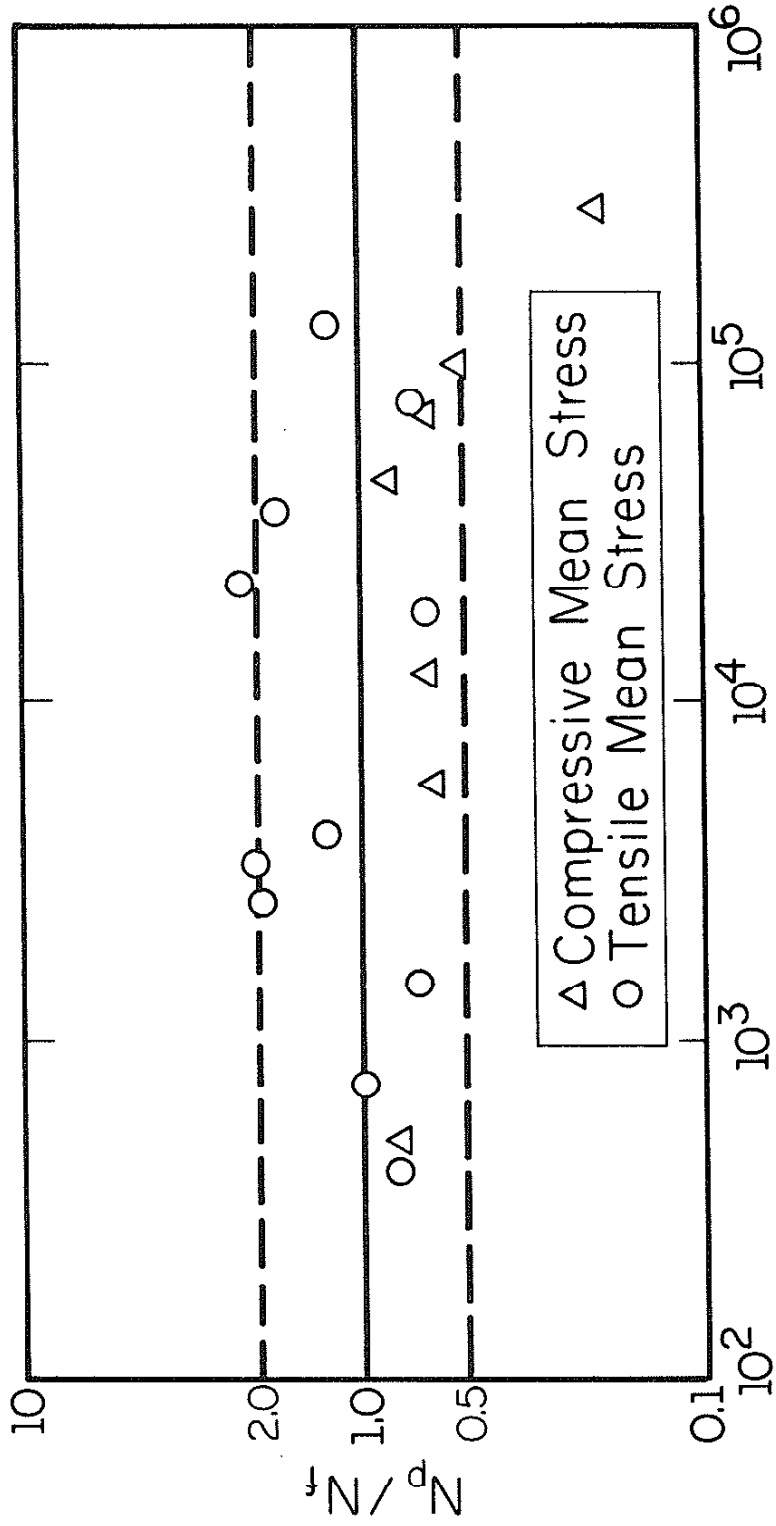

Figure 9. SWT Correlation of Uniaxial Fatigue Results

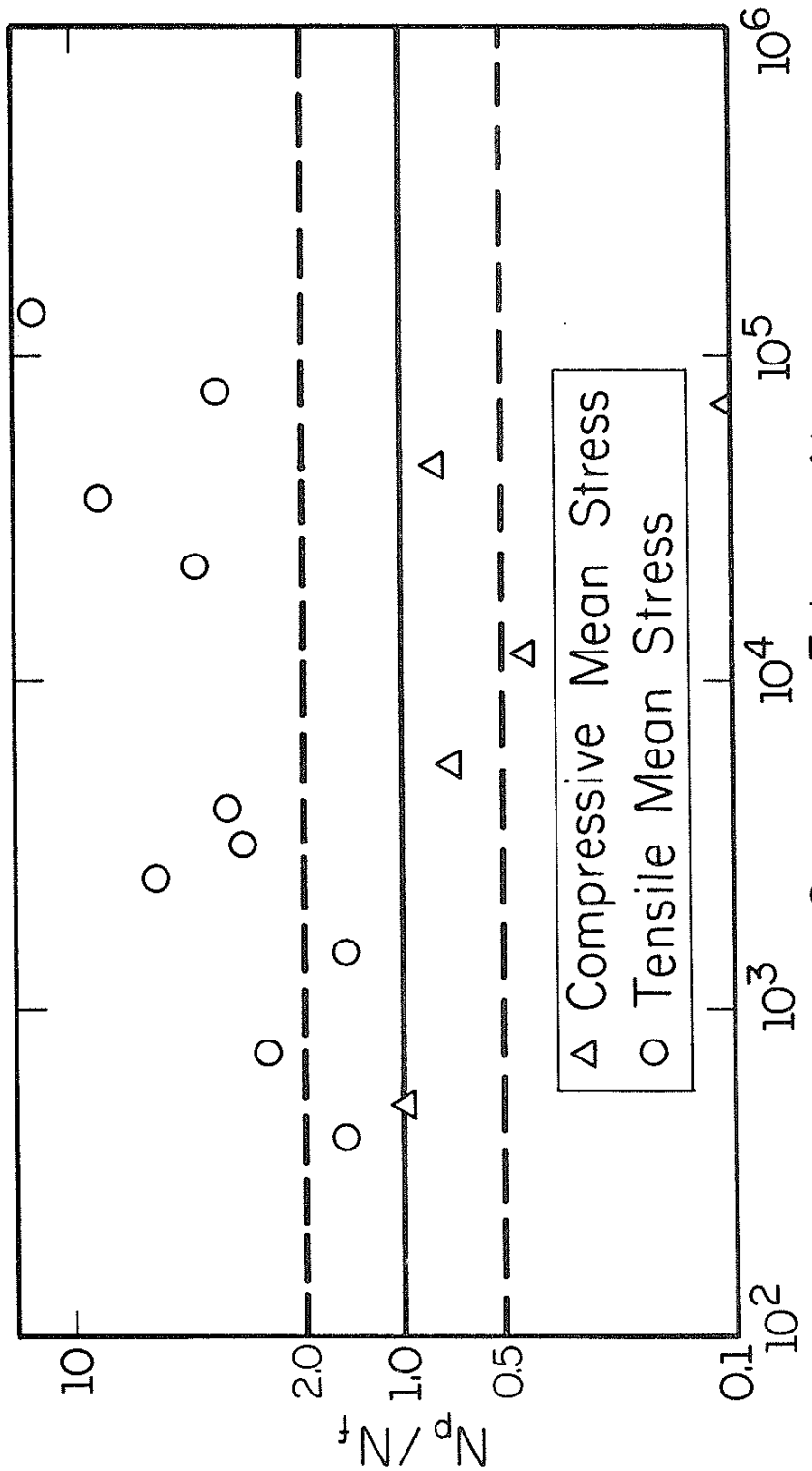

Figure 10. Manson-Halford Correlation of Uniaxial Fatigue Results

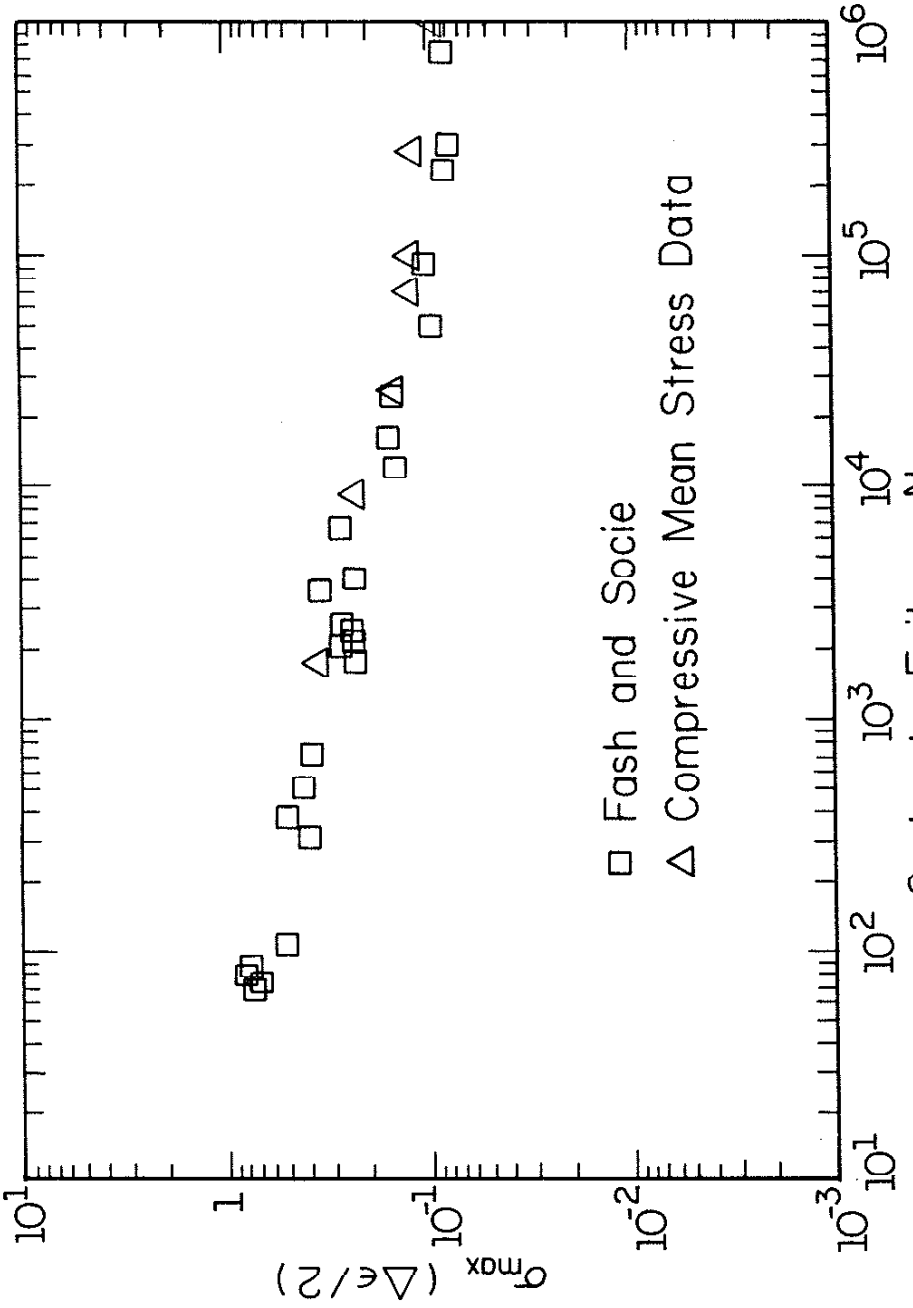

Figure 11. SWT Presentation of Mean Stress Fatigue Data

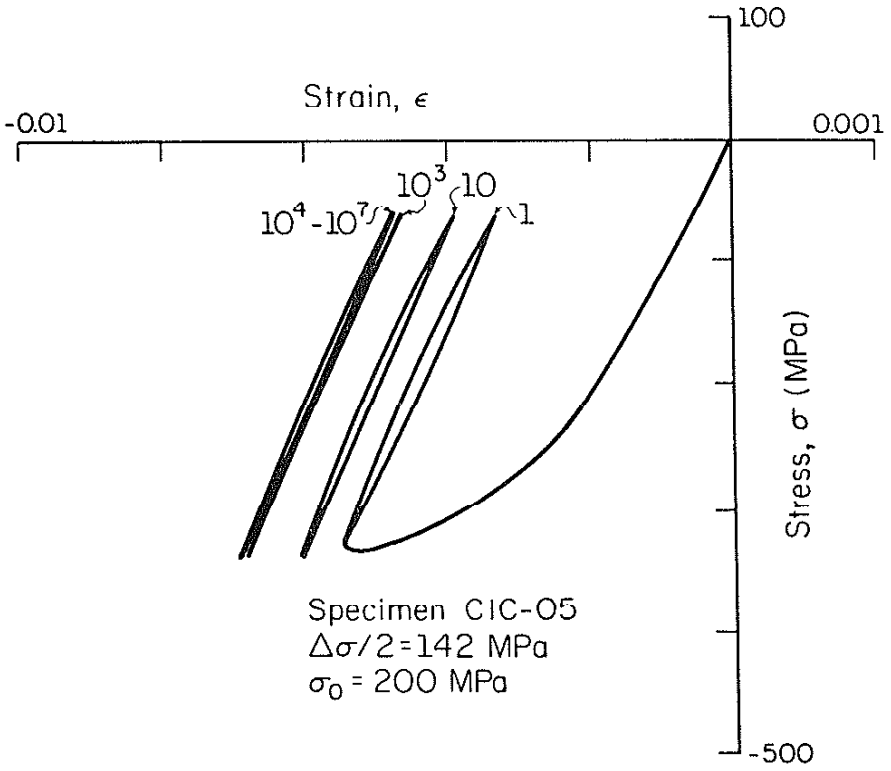

Figure 12. Stress-Strain Response of a Fully Compressive Load Control Test

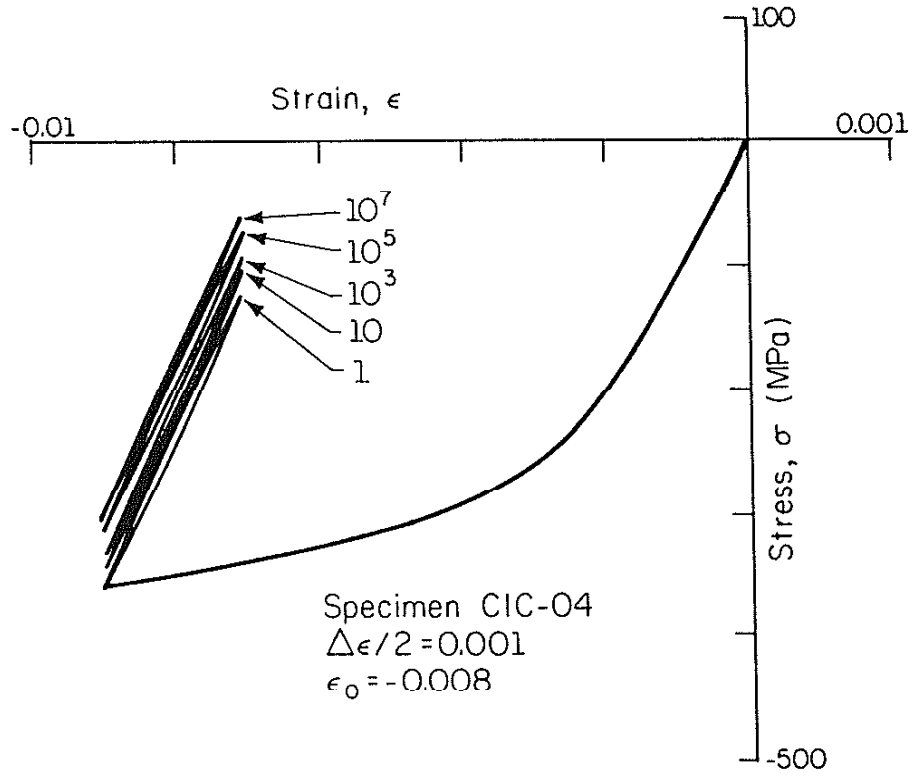

Figure 13. Stress-Strain Response of a Fully Compressive Strain Control Test

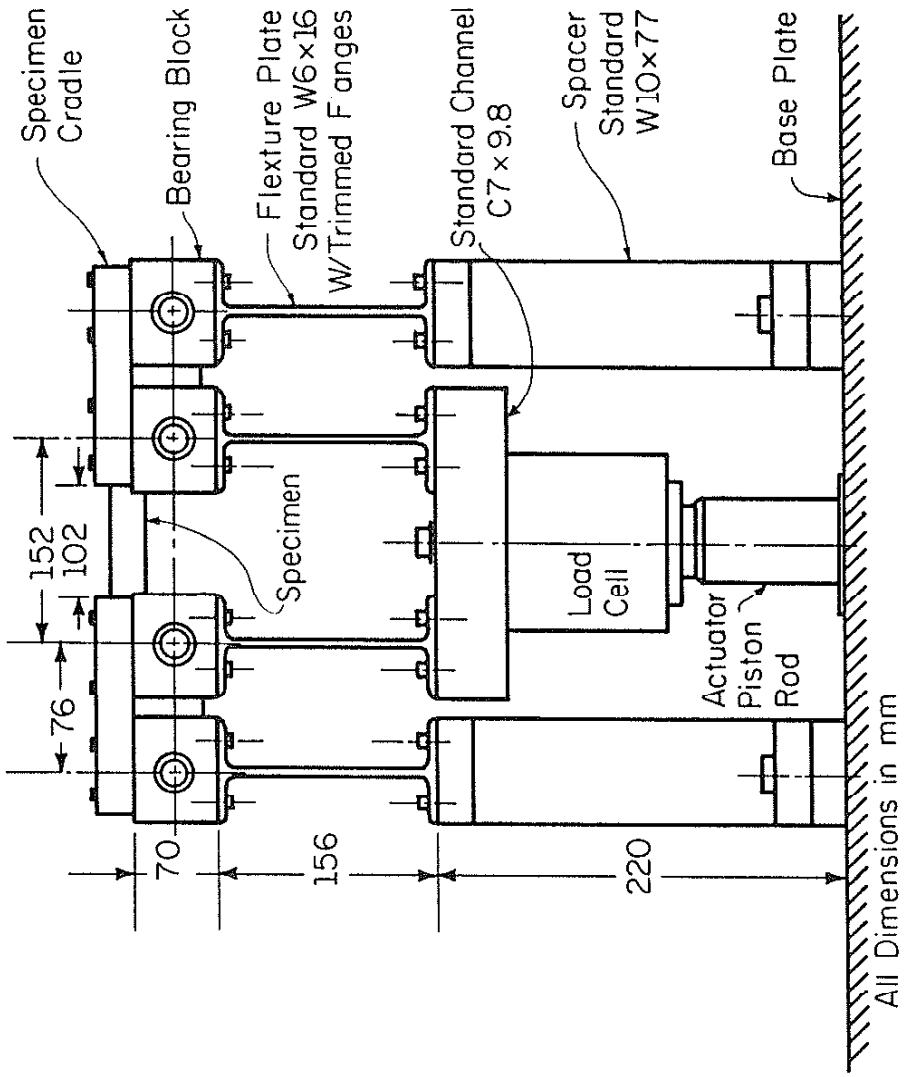

Figure 14. Four-Point Bending Test Fixture

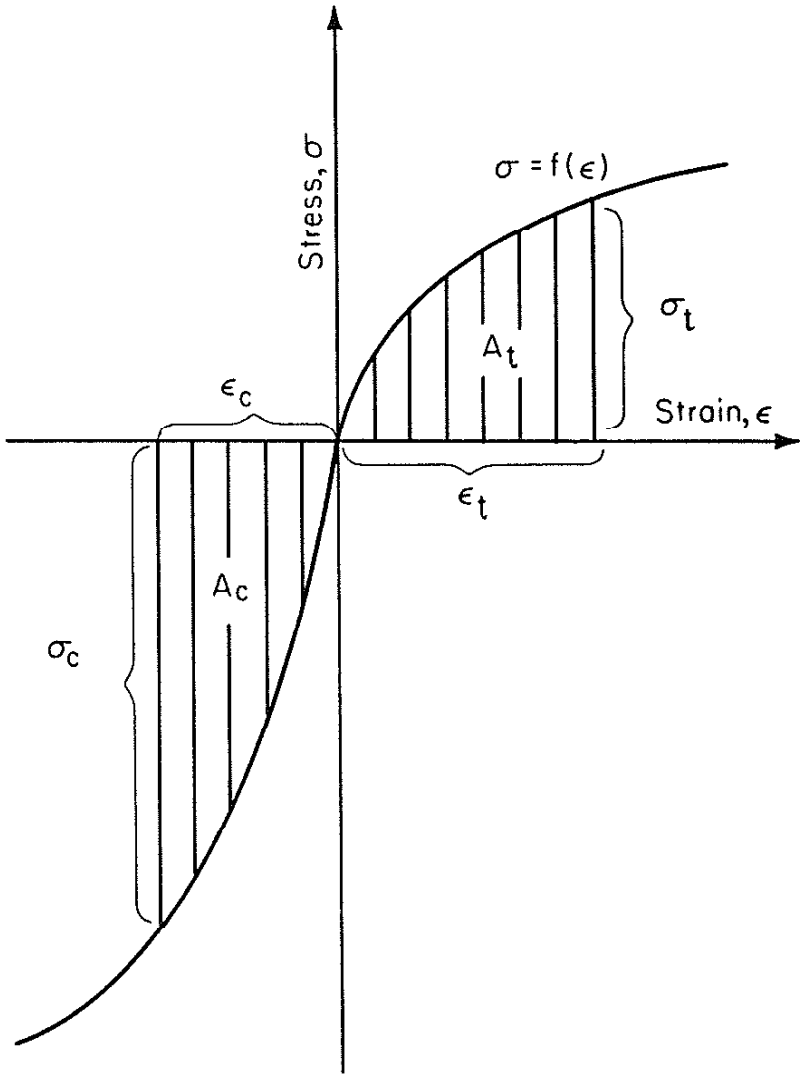

Figure 15. Equilibrium Strain Energy Formulation

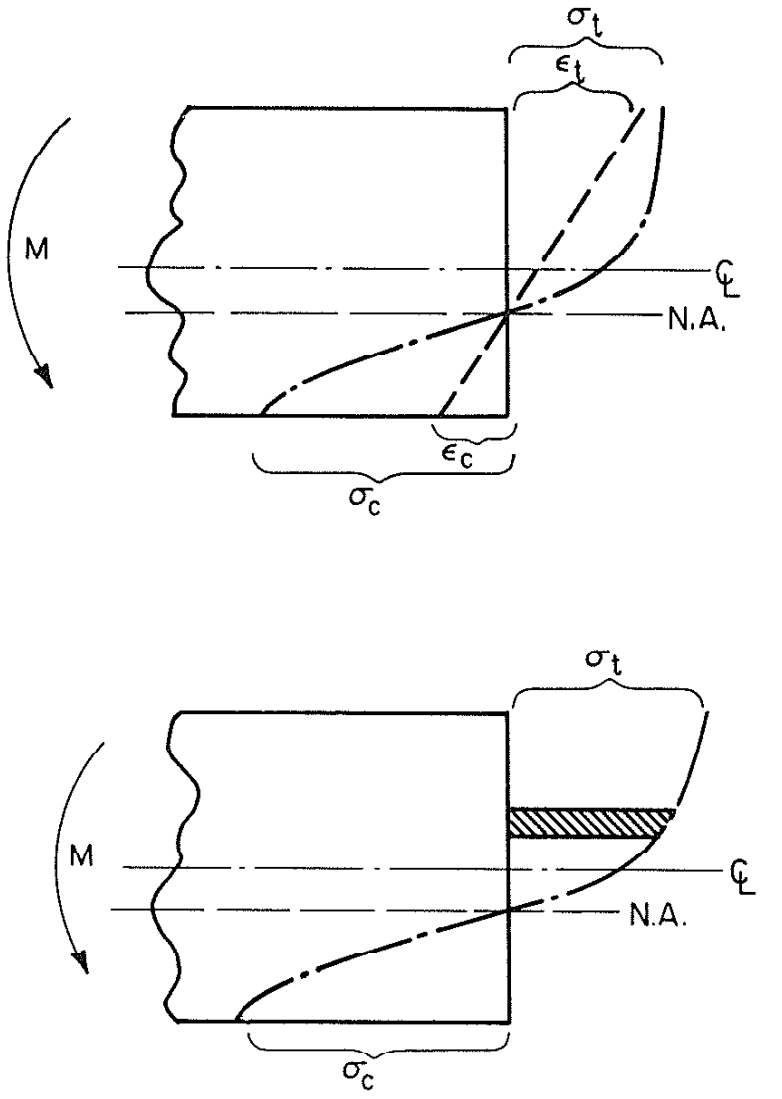

$$M = \sum \text{Force} \times \text{Moment Arm}_{\text{Tension}} + \sum \text{Force} \times \text{Moment Arm}_{\text{Compression}}$$

Figure 16. Relationship of Stress, Strain, and Moment

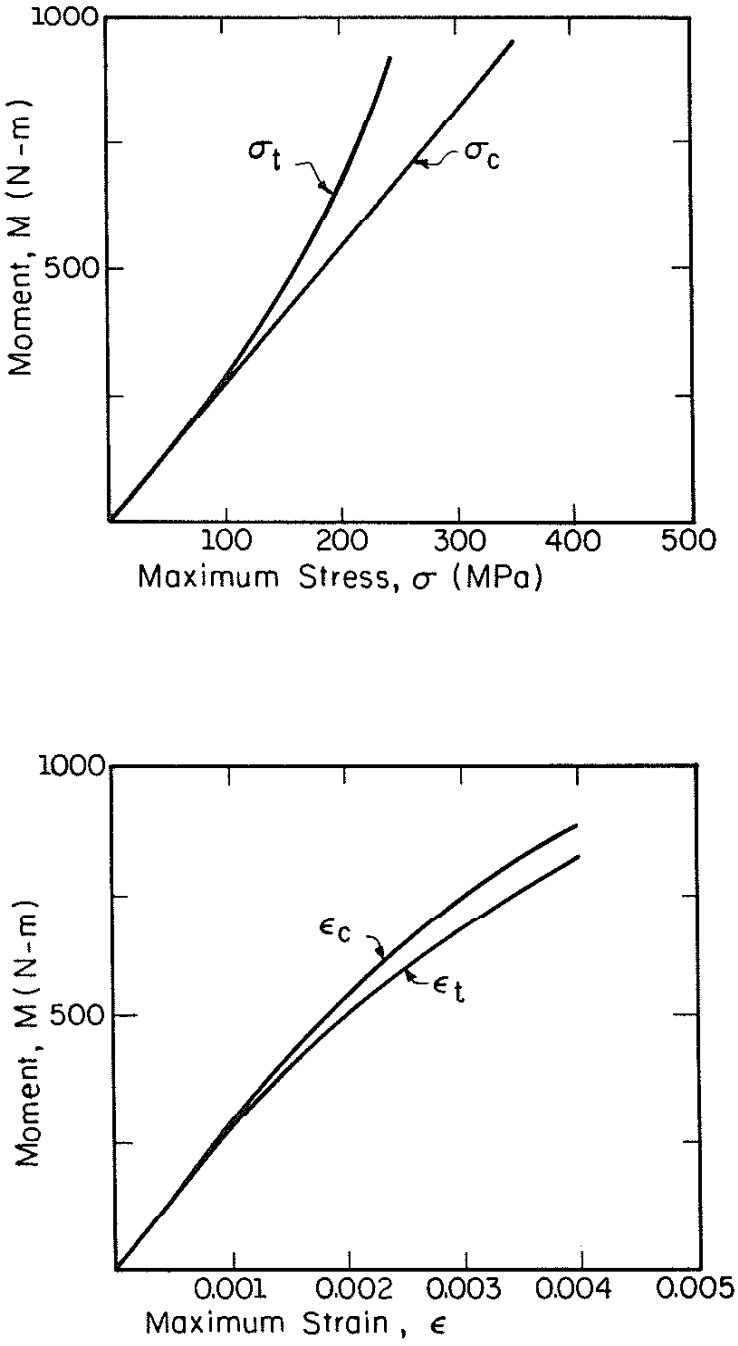

Figure 17. Moment-Maximum Stress and Moment-Maximum Strain Predictions

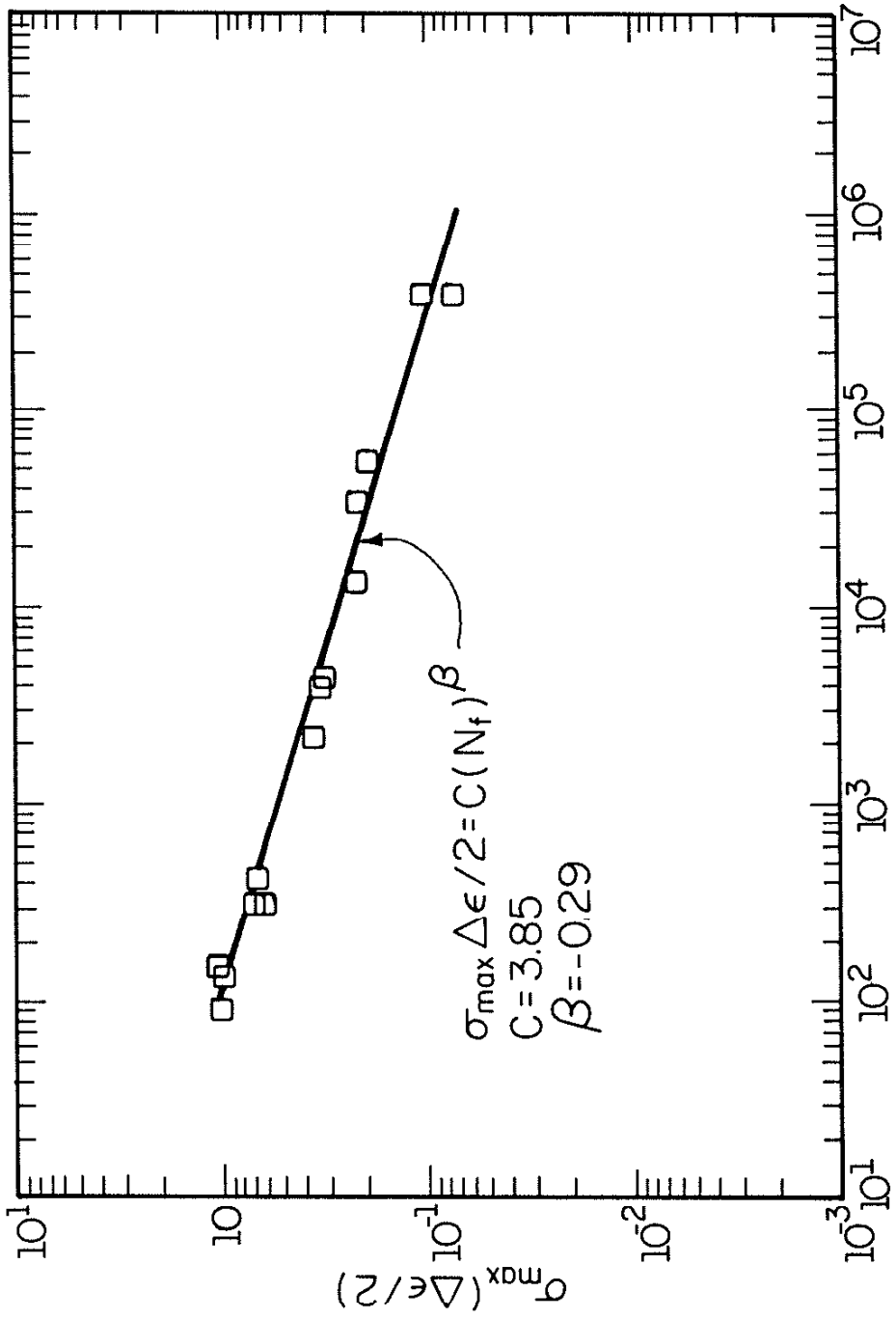

Figure 18. SWT Presentation of Strain-Life Fatigue Results Employed in the Bending Analysis

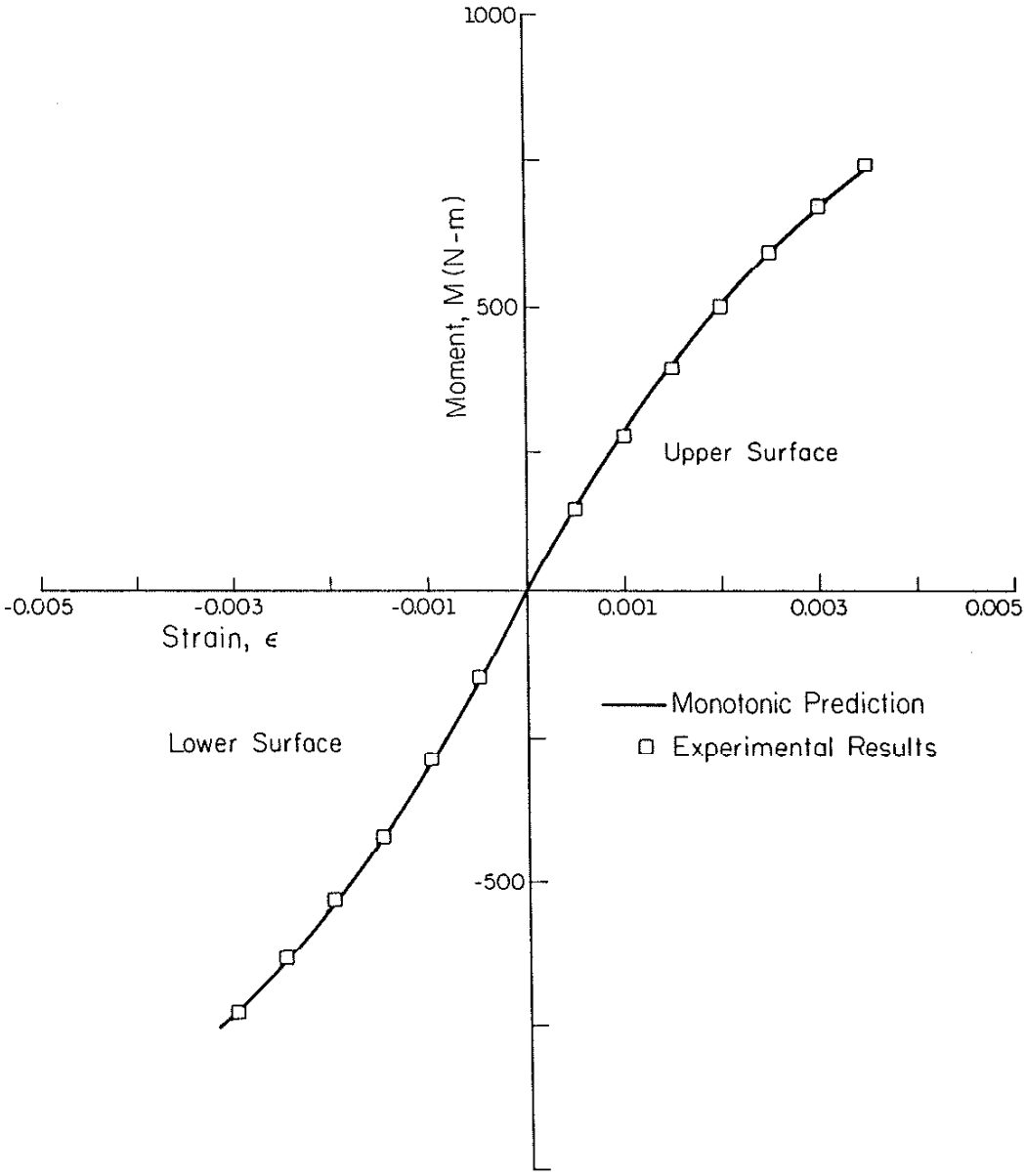

Figure 19. Flexural Monotonic Outer Fiber Moment-Strain Response

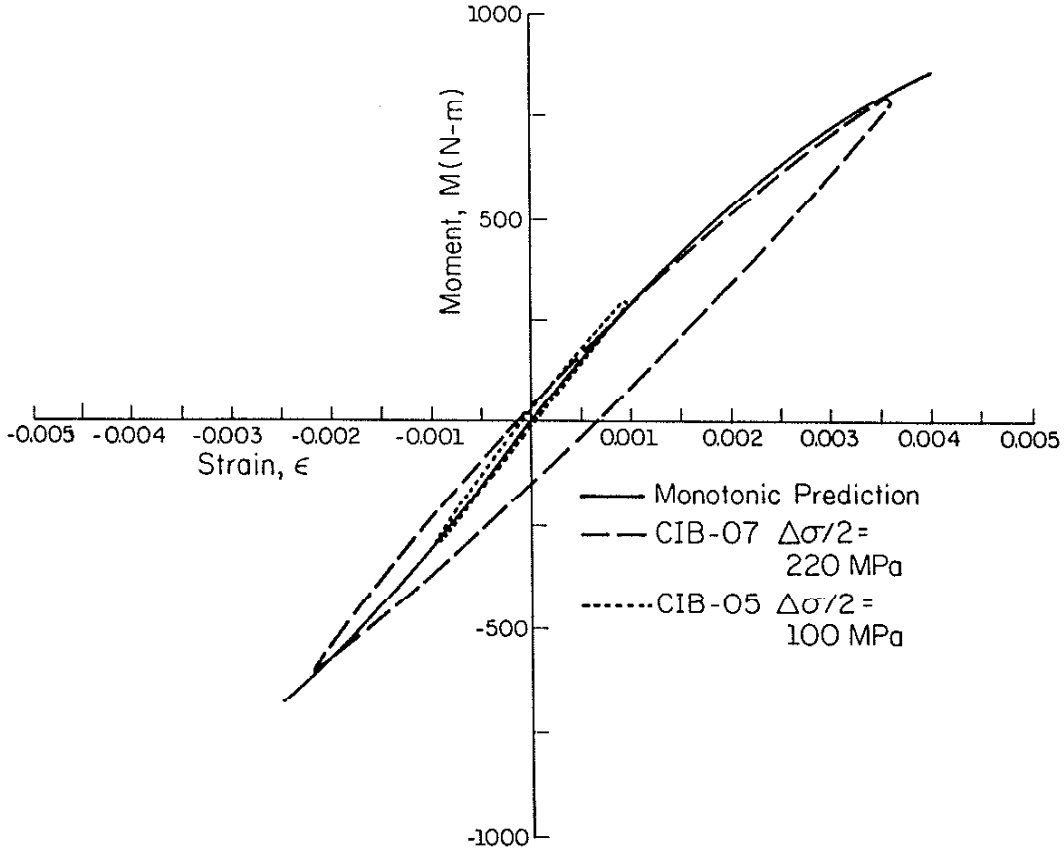

Figure 20. Cyclic Strain Amplitude Prediction

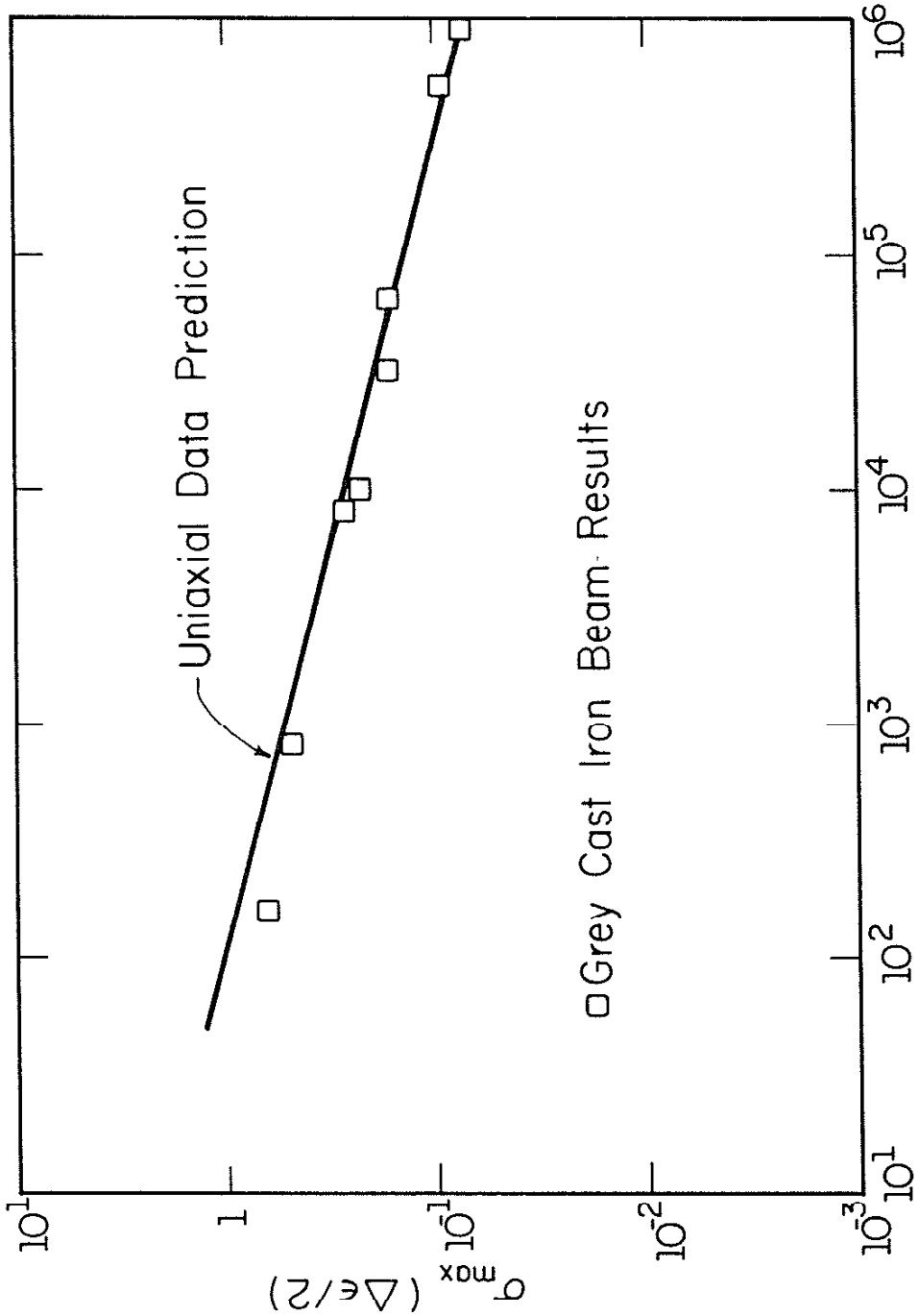

Figure 21. SWT Presentation of Bending Results

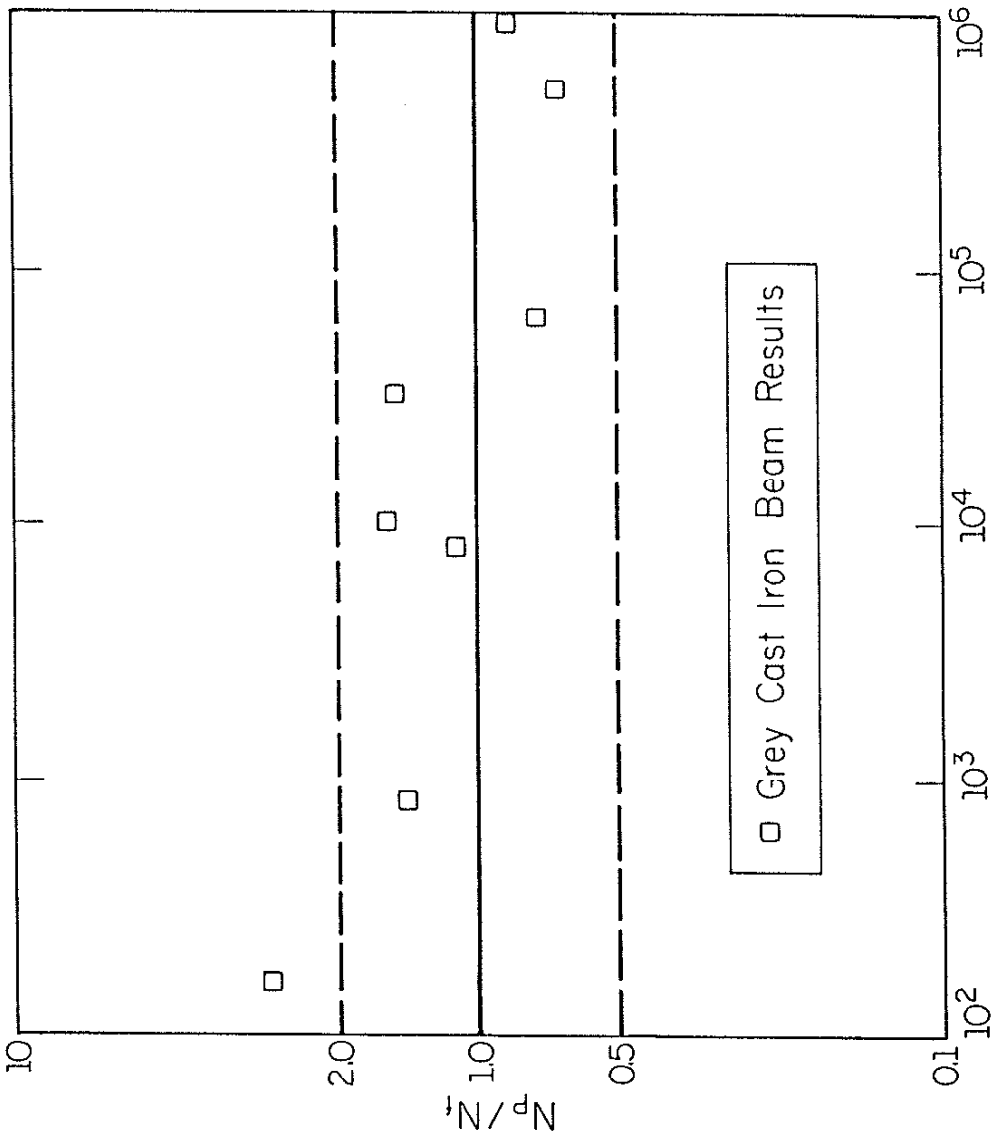

Figure 22. SWT Correlation of Beam Results

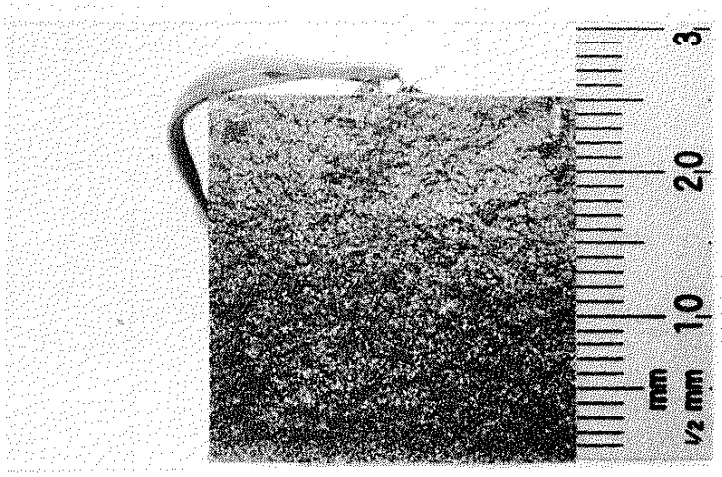

Figure 23. Beam Fracture Surface

APPENDIX I

Cyclic Deformation Model

A cyclic stress-strain model for constant or variable amplitude load histories was developed for cast iron by Downing [12]. Three factors were determined that affect cyclic deformation behavior of gray iron.

1. Symmetrical elastic/plastic response of the matrix and graphite constituents (termed bulk response).
2. Constraint effects around internal graphite flakes, transferring additional compressive stress to the matrix.
3. Debonding of surface graphite flakes, reducing tensile load capacity and allowing for greater strength in compression.

The relationship of these factors under cyclic loading was expressed as:

$$\sigma = A_{eff} (\sigma_B + \sigma_G) + (1 - A_{eff}) \sigma_{cc} \qquad (A1)$$

The effective area, A_{eff}, is a dimensionless parameter developed to reflect the fraction of cross-sectional area unaffected by surface cracking. Surface cracking is reflected in decreased unloading modulus; thus the effective area was expressed by

$$A_{eff} = E_u/E_o \quad . \qquad (A2)$$

Bulk stress-strain response was found to be dominated by the metal matrix. Characteristics similar to wrought metals were assumed to exist. Of primary significance were material memory (the occurrence of

closed hysteresis loops) and Masing behavior (where cyclic hysteresis loops are of the same form as initial loading curves if both the stresses and strains are multiplied by two). Bulk stresses, σ_B, were determined by

$$\varepsilon = \frac{\sigma_B}{E_o + m_B \sigma_B} + \left(\frac{\sigma_B}{k_B}\right)^{1/n_B} \qquad \text{(A3)}$$

Additional compressive stresses arising from graphite constraint effects, σ_G, were needed to reflect the assymetric stress-strain response. These increased compressive loads were expressed as:

$$\sigma_G = (\sigma_M)_c - (\sigma_B)_c \text{ if } \varepsilon \leq 0 \qquad \text{(A4)}$$

and

$$\sigma_G = 0 \qquad \text{if } \varepsilon > 0 \quad . \qquad \text{(A5)}$$

Graphite stress was considered to be nonlinear elastic and only dependent on compressive strain.

Crack closure stress, σ_{cc}, was also developed to model a portion of the assymetric stress-strain behavior. At some point during unloading, open surface cracks close, resulting in additional load transmitting area. Compressive stresses due to crack closure were considered to be nonlinear elastic and represented by

$$\sigma_{cc} = Q(\varepsilon_{max} - \varepsilon)^q \qquad \text{(A6)}$$

where Q and q new material constants obtained from the monotonic material properties and strain limits.

APPENDIX II

Strain-Life Fatigue Data

Results from completely reversed strain controlled fatigue tests of a gray cast iron are presented. This previously unreported work was conducted by P. Kurath, J. Fash, and D. Socie at the Materials Engineering Research Laboratory, University of Illinois at Urbana-Champaign, Urbana, IL. SWT presentation of the data is illustrated in Fig. 18.

Specimen No.	$\Delta\varepsilon/2$	$N_{10\%}$	N_f	σ_{max}(MPa)
10	0.001	376,780	1.049×10^6	104.9
20	0.001	---	1.032×10^6	66.5
1	0.0015	52,186	52,186	124.2
8	0.0015	32,768	38,823	142.8
11	0.0015	12,845	37,978	141.7
3	0.002	3,825	7,610	157.1
5	0.002	4,258	8,061	158.5
19	0.002	2,049	5,749	167.5
2	0.003	408	938	201.6
6	0.003	303	896	208.5
9	0.003	303	503	198.9
4	0.004	129	131	233.8
7	0.004	146	172	263.9
12	0.004	88	100	239.3

REFERENCES

1. Morrow, J. D., and Socie, D. F., "The Evolution of Fatigue Crack Initiation Life Prediction Methods," Experimentation and Design in Fatigue, Proceedings of Fatigue 1981, F. Sherratt and J. B. Sturgeon, eds., Society of Environmental Engineers, Warwick University, England, Westbury House, 1981, pp. 1-21.

2. Socie, D. F., "Fatigue Life Prediction Using Local Stress-Strain Concepts," Experimental Mechanics, Vol. 17, No. 2, 1977, pp. 50-56.

3. "Standard Recommended Practice for Constant-Amplitude Low-Cycle Fatigue Testing, E606-80," 1984 Annual Book of ASTM Standards, Section 3, Vol. 3.01 Metals Test Methods and Analytical Procedures, American Society for Testing and Materials, 1984, pp. 653-670.

4. Thum, A., and Ude, H., "Die Elastizitat und die Sahwingungsfestigkeit des Gusseisens," Die Giesserei, Vol. 16, 1929, pp. 547-556.

5. Gilbert, G. N. J., "Variation of Microstructure of a Flake Graphite Cast Iron after Stressing in Tension and Compression," Journal of the British Cast Iron Research Association, Vol. 12, 1954, pp. 31-47.

6. Ikawa, K., and Ohira, G., "Fatigue Properties of Cast Iron in Relation to Graphite Structure," American Foundry Society, Cast Metals Research Journal, Vol. 3, No. 1, 1967, pp. 11-21.

7. Mitchell, M. R., "Effects of Graphite Morphology, Matrix Hardness, and Structure on the Fatigue Resistance of Gray Cast Iron," Society of Automotive Engineers, Inc., Report No. 750198, 1975, 13 pp.

8. Fash, J. W., Socie, D. F., and Russell, E. F., "Fatigue Crack Initiation and Growth in Gray Cast Iron," Experimentation and Design in Fatigue, Proceedings of Fatigue 1981, F. Sherratt and J. B. Sturgeon, eds., Society of Environmental Engineers, Warwick University, England, Westbury House, 1981, pp. 40-41.

9. Fash, J. W., and Socie, D. F., "Fatigue Behavior and Mean Effects in Gray Cast Iron," Int. Journal of Fatigue, Vol. 4, No. 3, 1982, pp. 137-142.

10. Smith, K. N., Watson, P., and Topper, T. H., "A Stress-Strain Function for the Fatigue of Metals," Journal of Materials, Vol. 5, No. 4, Dec. 1970, pp. 767-778.

11. Socie, D. F., Fash, J. W., and Leckie, F. A., "A Continuum Damage Model for Fatigue Analysis of Cast Iron," Proceedings of the ASME International Conference on Advances in Life Prediction Methods, D. A. Woodford and J. R. Whitehead, eds., The American Society of Mechanical Engineers, Albany, New York, 1983, pp. 59-64.

12. Downing, S. D., "Modeling Cyclic Deformation and Fatigue Behavior of Cast Iron Under Uniaxial Loading," Materials Engineering Mechanical Behavior Report No. 101 (UICU-ENG 84-3601), 1984, 106 pp.

13. "Standard Method for Evaluating the Microstructure of Graphite in Iron Casting, A247," 1983 Annual Book of ASTM Standards, Section 1, Vol. 1.02, Ferrous Castings, American Society for Testing and Materials, 1983, pp. 133-135.

14. Morrow, J., Section 3.2 of Fatigue Design Handbook, Society of Automotive Engineers Advances in Engineering, Vol. 4, 1968, pp. 21-29.

15. Basquin, O. H., "The Exponential Law of Endurance Tests," Proceedings of the American Society for Testing Materials, Vol. 10, 1910, pp. 625-630.

16. Manson, S. S., and Halford, G. R., "Practical Implementation of the Double Linear Damage Rule and Damage Curve Approach for Treating Cumulative Fatigue Damage," Int. Journal of Fracture, Vol. 17, No. 2, 1981, pp. 169-172, R35-R42.

17. Bach, C., and Baumann, R., Elastizitat und Festigkeit, 9th ed., Julius Springer, Berlin, 1924.

18. Meyer, Eugen, "The Calculation of the Deflection of Bars Whose Material Does Not Follow Hooke's Law," zeit. V.D.I., Vol. 52, 1908, pp. 167-173.

19. Nadai, A., Theory of Flow and Fracture of Solids, McGraw-Hill Book Company Inc., Vol. 1, 1950, pp. 353-370.